Astron. Astrophys. 349, 649–659 (1999)

ASTRONOMY
AND
ASTROPHYSICS

CCD photometry of distant comets

S.C. Lowry[1], **A. Fitzsimmons**[1], **I.M. Cartwright**[1], **and I.P. Williams**[2]

[1] APS Division, Department of Pure and Applied Physics, The Queen's University of Belfast, Belfast BT7 1NN, UK
[2] Astronomy Unit, School of Mathematical Sciences, Queen Mary and Westfield College, Mile End Road, London E1 4NS, UK

Received 25 January 1999 / Accepted 19 July 1999

Abstract. While it is apparent that many comets are active beyond the canonical distance of 3 AU, few surveys of cometary activity have been performed in this region previously. Such a survey enables a more accurate determination of the proportion of comets that exhibit little or no outgassing at these distances. Results are presented of CCD observations of comets in the region of 3 AU $\leq$ R_h $\leq$ 6 AU obtained with the 1m JKT on La Palma. Photometric observations of 15 comets were obtained, 7 of which displayed coma activity and 8 of which appeared inactive. BVR photometry was performed on these comets to determine dimensions, colours and outgassing rates. Although 40P/Vaisala 1 and 26P/Grigg-Skjellerup were not detected, upper limits to their nuclear radii are presented. The results obtained are compared with previous observations.

Key words: techniques: photometric – comets: general

1. Introduction

An understanding of the physical properties of cometary nuclei and their size distribution is important to constrain early solar system models. Unfortunately cometary nuclei are extremely difficult to observe. They can only be observed at large heliocentric distances where the sublimation of surface volatiles is so low that any photometric measurements made are dominated by light reflected from the nucleus rather than from the dust coma whose scattering cross-section dominates the observed flux at small heliocentric distances. Nucleus size estimates have continued to decrease as more effective techniques emerge which are able to quantify the coma contamination. With the exception of the Centaur (2060) Chiron and C/1995 O1 (Hale-Bopp), modern measurements of nuclear radii range from 0.3 km $<$ r_N $<$ 11.8 km (Meech 1998 and references therein; Mueller 1992; Hainaut et al. 1998).

From recent work it is evident that comets exhibit coma activity at larger heliocentric distances than previously believed (Meech 1994). For example C/1995 O1 (Hale-Bopp) possessed a dust coma at $R_h = 13.1$ AU (McNaught & Cass 1995). Also Chiron was seen to display considerable activity near aphelion (at $R_h = 17.8$–18.8 AU) using pre-discovery photographic plate images taken between 1969–1977 (Bus et al. 1998). In fact this aphelion activity substantially exceeded, both in degree and duration, the observed activity as Chiron approached its most recent perihelion passage. Such observations have important implications. For example if comets are active throughout their entire orbit it would mean that their nuclei are being continuously resurfaced. The observed diversity of nucleus colours (Luu 1993) could be a result of this. Also if the total mass loss rate per orbit is underestimated then the total lifetimes of cometary nuclei would tend to be overestimated.

Few studies of distant comets have been carried out in the past. Meech & Hainaut (1997) have an on-going long-term programme to obtain CCD images of short and long period comets over a wide range of heliocentric distances to compare activity levels and obtain information about primordial and evolutionary differences between comets with different dynamical histories. The largest study of cometary activity to date was by A'Hearn et al. (1995), but in this study only $\sim$ 3% of the observations were at a heliocentric distance $>$ 3 AU. We describe in this paper observations of distant comets that were obtained in order to increase our knowledge of activity in this region.

2. Observations and reduction

CCD imaging of comets in the range 3 AU $\leq$ R_h $\leq$ 6 AU was carried out between 24th & 31st August 1995 using the 1-m Jacobus Kapteyn Telescope on the Island of La Palma. Only the first 4 nights were photometric. Table 1 lists the observational circumstances for each comet observed. A TEK 1024×1024 pixel CCD was used at the f/15 cassegrain focus resulting in an image scale of 0.33 arcsec per pixel. A log of all cometary observations is listed in Table 2. All images were taken through one of the RGO Harris R & V filters and the KPNO B filter. All cometary images were obtained with the telescope tracking at the sidereal rate with the exception of 86P/Wild 3 and 120P/Mueller 1 which were differentially tracked at their respective apparent motions. A number of observations of the standard field SA92 (Landolt 1992) in all 3 filters were taken throughout the 4 nights along with bias and twilight flat field exposures for the calibration of the images. Counts from the standard stars were measured

Send offprint requests to: Stephen.Lowry@qub.ac.uk
Correspondence to: Stephen.Lowry@qub.ac.uk

Table 1. Observational geometry for all comets. R_h and Δ are the heliocentric and geocentric distances respectively. α is the phase angle.

Comet	R_h [AU]	Δ [AU]	α [deg.]
9P/Tempel 1	3.511	2.935	14.9
26P/Grigg−Skjellerup	4.772	4.496	12.0
32P/Comas−Solá	3.089	2.413	15.8
40P/Vaisala 1	6.007	5.001	1.1
43P/Wolf−Harrington	4.869	4.256	10.1
69P/Taylor	4.886	3.989	6.1
74P/Smirnova−Chernykh	4.610	3.736	7.0
79P/du Toit−Hartley	4.739	4.285	11.5
81P/Wild 2	4.246	4.002	12.5
86P/Wild 3	3.350	2.454	9.3
87P/Bus	3.384	2.437	7.1
89P/Russell 2	3.041	2.406	16.7
119P/Parker−Hartley	3.421	2.657	12.6
120P/Mueller 1	3.079	2.077	2.9
P/1993 K2 (Helin−Lawrence)	4.696	4.003	9.8

through apertures of 6.6 arcsec radii in order to conform with apertures used by Landolt (1992) and converted to instrumental magnitudes. Atmospheric extinction coefficients for the B, V, and R filters were then calculated for each of the 4 photometric nights. For comets with only R band imaging, we found that the uncertainty introduced when assuming a comet colour in the conversion of instrumental to apparent magnitudes was negligible. Object detection was achieved by their known motion relative to the background stars. Detection was immediate in some cases but for others such as 43P/Wolf-Harrington several images were shifted and then coadded to give a larger signal to noise ratio. Image processing and photometry was performed with the IRAF/CCDRED (Massey 1997), IRAF/APPHOT (Davis 1989) & IRAF/DAOPHOT (Davis 1994) packages on the Northern Ireland STARLINK node.

3. Results and analysis

The techniques used to analyse these data varied, depending on the observed appearance of the comet. Hence we describe separately the results and analysis for the undetected, unresolved and active comets.

3.1. Undetected comets

• *40P/Vaisala 1 & 26P/Grigg−Skjellerup*
For each comet the corresponding images were shifted and coadded using their known rates of motion in an attempt to reveal the objects by increasing the signal to noise ratio. The objects remained undetected. Limiting magnitudes were determined by adding artificial stars at certain positions to the individual frames. The frames were then blinked to simulate the motion of the comet between frames. The magnitude of the artificial stars were gradually decreased until they were no longer detectable, by visual inspection, against the background noise. This iterative process eventually determined limiting magnitudes down to an accuracy of 0.1 magnitudes. As the images of 40P/Vaisala 1 & 26P/Grigg−Skjellerup were obtained with sidereal tracking a small correction must be applied to the limiting magnitude due to trailing of the comets during the exposures (see Fig. 3 of Tancredi et al. 1994). The corrected limiting magnitudes are given in Table 3. Taking these limiting magnitudes as the upper limit to the comet brightness, upper limits to their nuclear radii were derived using the following expression (Russell 1916):

$$A_R C = \frac{2.25 \times 10^{22} R_h^2 \pi \Delta^2 10^{0.4(m_\odot - m_\mathrm{R})}}{10^{-0.4\alpha\beta}} \quad (1)$$

where R_h[AU] and Δ[AU] are the heliocentric and geocentric distances respectively, C[m^2] is the geometrical cross-section of the nucleus, $m_\odot$ and m_R are the apparent R magnitudes of the sun and comet respectively. A_R is the geometric albedo in the R filter, which throughout this paper is assumed to be 4% (see Fig. 6 of Fitzsimmons et al. 1994, and references therein). The denominator expresses the phase angle dependence of the brightness where α and β are the phase angle and phase coefficient respectively. Throughout this paper a value of 0.04 for β is taken from previous studies (Luu & Jewitt 1992).

3.2. Unresolved comets

• *69P/Taylor, 81P/Wild 2, 43P/Wolf−Harrington, 120P/Mueller 1, 86P/Wild 3 & 79P/du Toit−Hartley*
All images in this section were taken through the R filter. Nearby stars were removed from all exposures of these six comets using the IRAF/DAOPHOT package. The average point spread function (PSF) of the background stars was calculated and fitted to the contaminant stars which were then subsequently removed using the `substar` task. The analysis procedure was similar for all comets in this section. Therefore for reasons of clarity we describe just the analysis of 69P/Taylor in detail.

All exposures of the comet were shifted and coadded. The average airmass was used in the calculation to convert instrumental magnitudes to apparent magnitudes. To determine whether the comet had a resolved coma the PSF for the combined frame was subtracted from the image of the comet. This process completely removed the comet from the frame and it was therefore regarded as a point source. The absence of any residual flux after PSF subtraction shows that any trailing of the comet is negligible. Indeed this was the case for all the sidereally tracked unresolved comets. The apparent magnitude was measured and substituted into Eq. (1) to calculate the nuclear radius. Both values are listed in Table 3.

To quantify any coma contribution to the magnitude the following expression is applied (Jewitt & Danielson 1984):

$$m_\mathrm{coma} = \Sigma(r) - 2.5\log(2\pi r^2) \quad (2)$$

where m_coma is the integrated magnitude of the assumed steady state coma within a circular aperture of radius r[arcsec] and $\Sigma(r)$[mag./arcsec^2] is the measured brightness at r. To calculate an upper limit for $\Sigma(r)$ the following approach is used. For faint

Table 2. B, V, & R filter observations for all comets. All images were obtained with the telescope tracking at the sidereal rate unless otherwise stated.

Comet	Date	UT (start of exposure)	Filter	Airmass	Exposure time [s]	Extinction coefficient	Colour coefficient
9P/Tempel 1	1995 Aug.	27.108	R	1.426	600	0.091 ± 0.007	0.013 ± 0.012
		27.133	R	1.278	600		
		27.158	V	1.184	600	0.116 ± 0.014	0.007 ± 0.015
		27.167	B	1.159	600	0.231 ± 0.016	-0.053 ± 0.015
26P/Grigg−Skjellerup	1995 Aug.	28.147	R	1.323	900	0.095 ± 0.019	-0.026 ± 0.012
		28.174	R	1.187	900		
32P/Comas−Sola	1995 Aug.	25.069	R	1.795	600	0.086 ± 0.005	0.016 ± 0.09
		25.085	V	1.604	600	0.021 ± 0.006	0.007 ± 0.011
		25.094	B	1.521	600	0.201 ± 0.100	-0.056 ± 0.017
40P/Vaisala 1	1995 Aug.	24.932	R	1.869	300	0.086 ± 0.005	0.011 ± 0.016
		24.956	R	1.649	300		
		24.980	R	1.516	300		
43P/Wolf−Harrington	1995 Aug.	24.906	R	1.346	600	0.086 ± 0.005	0.011 ± 0.016
		24.940	R	1.423	600		
69P/Taylor	1995 Aug.	26.950	R	1.874	300	0.091 ± 0.007	0.013 ± 0.012
		26.970	R	1.840	300		
74P/Smirnova−Chernykh	1995 Aug.	25.975	R	1.754	300	0.078 ± 0.011	0.009 ± 0.014
		25.988	R	1.779	300		
		25.994	V	1.795	300	0.123 ± 0.011	-0.013 ± 0.011
		26.000	B	1.815	300	0.185 ± 0.017	-0.058 ± 0.014
79P/du Toit−Hartley	1995 Aug.	25.150	R	1.130	900	0.086 ± 0.005	0.011 ± 0.016
		25.194	R	1.037	900		
81P/Wild 2	1995 Aug.	26.197	R	1.075	900	0.078 ± 0.011	0.009 ± 0.014
		26.224	R	1.045	900		
86P/Wild 3†	1995 Aug.	28.116	R	1.517	900	0.095 ± 0.019	-0.026 ± 0.012
		28.131	R	1.498	900		
87P/Bus	1995 Aug.	24.919	R	1.550	300	0.086 ± 0.005	0.011 ± 0.016
		24.949	R	1.442	300		
		24.998	R	1.408	300		
		25.010	V	1.430	300	0.121 ± 0.006	0.007 ± 0.011
		25.017	V	1.445	300		
89P/Russell 2	1995 Aug.	26.085	R	1.520	900	0.078 ± 0.011	0.009 ± 0.014
		26.151	R	1.165	900		
		26.183	V	1.105	900	0.123 ± 0.011	-0.013 ± 0.011
119P/Parker−Hartley	1995 Aug.	25.026	V	1.546	600	0.121 ± 0.006	0.007 ± 0.011
		25.035	R	1.458	600	0.086 ± 0.005	0.011 ± 0.016
		25.044	B	1.384	600	0.201 ± 0.100	-0.056 ± 0.017
120P/Mueller 1†	1995 Aug.	28.008	R	1.474	300	0.095 ± 0.019	-0.026 ± 0.012
		28.019	R	1.429	600		
		28.031	R	1.391	600		
P/1993 K2 (Helin−Lawrence)	1995 Aug.	25.079	R	1.555	300	0.086 ± 0.005	0.011 ± 0.016
		25.105	R	1.374	600		
		25.127	B	1.273	600	0.201 ± 0.100	-0.056 ± 0.017
		25.174	B	1.171	600		
		25.137	V	1.241	600	0.121 ± 0.006	0.007 ± 0.011
		25.183	V	1.165	600		

† Differentially tracked

objects the signal to noise ratio (S/N) is given by the usual formula:

$$S/N = \frac{I.t}{\sqrt{n}.\sigma} \quad (3)$$

where n is the number of pixels within the aperture, I is the total measured intensity [ADU's/sec] of the object within the aperture, t is the exposure time and σ is the standard deviation of the background noise. By assuming that S/N should be at least 2 for the comet to be detectable[1], then a minimum value for the brightness/arcsec^2 can be obtained and substituted for

[1] The choice of 2 for S/N was shown to be appropriate by Hainaut et al. (1994).

Table 3. R magnitude and radii estimates for the inactive comets. Lower limits for $m_{\rm coma}$, the steady state coma magnitude, are derived using Eq. (2).

Comet	R Magnitude	Radius [km]	$m_{\rm coma}$	$Af\rho$ [cm] based on $m_{\rm coma}$
40P/Vaisala 1	$21.7 \pm 0.1^{\dagger}$	$\leq 3.6 \pm 0.2$	–	–
26P/Grigg−Skjellerup	$23.7 \pm 0.1^{\dagger}$	$\leq 1.2 \pm 0.1$	–	–
69P/Taylor	21.0 ± 0.4	3.6 ± 0.7	≥ 21.84	≤ 13.6
81P/Wild 2	22.3 ± 0.3	2.0 ± 0.3	≥ 21.86	≤ 12.1
43P/Wolf−Harrington	21.4 ± 0.5	3.3 ± 0.7	≥ 21.48	≤ 28.4
120P/Mueller 1	20.3 ± 0.2	1.5 ± 0.2	≥ 20.76	≤ 9.1
86P/Wild 3	21.7 ± 0.3	1.1 ± 0.2	≥ 22.01	≤ 4.0
79P/du Toit−Hartley	23.3 ± 0.4	1.4 ± 0.3	≥ 21.55	≤ 21.6

† Limiting magnitudes

Table 4. B,V & R magnitudes for the active comets.

Comet	B	V	R	B−V	V−R
119P/Parker−Hartley	18.74 ± 0.10	17.92 ± 0.06	17.40 ± 0.05	0.82 ± 0.12	0.52 ± 0.08
32P/Comas−Solá	19.25 ± 0.10	18.43 ± 0.06	17.86 ± 0.06	0.82 ± 0.12	0.57 ± 0.08
74P/Smirnova−Chernykh	18.79 ± 0.14	17.80 ± 0.08	17.36 ± 0.06	0.99 ± 0.16	0.44 ± 0.10
P/1993 K2 (Helin−Lawrence)	20.29 ± 0.12	19.94 ± 0.09	19.17 ± 0.08	0.35 ± 0.15	0.77 ± 0.12
9P/Tempel 1	20.64 ± 0.21	20.18 ± 0.18	19.81 ± 0.12	0.46 ± 0.28	0.37 ± 0.22
89P/Russell 2	–	20.70 ± 0.24	19.82 ± 0.13	–	0.88 ± 0.27
87P/Bus	–	19.75 ± 0.14	19.86 ± 0.16	–	-0.11 ± 0.21

$\Sigma(r)$ in Eq. (2). r is taken to be the point where the PSF for the combined frames becomes negligible i.e. at $\sim$ 2% of its peak intensity. Applying this to 69P/Taylor yields $m_{\rm coma} \geq 21.84$. The measured total magnitude was 21.0 ± 0.4. From this it can be said that the nucleus significantly dominates the observed flux.

This same procedure was repeated for all exposures of 81P/Wild 2 and 43P/Wolf-Harrington. Unfortunately in the case of 86P/Wild3 and 120P/Mueller 1 background stars were trailed therefore a slightly different method is used to compare the PSF of the background stars with the cometary profiles. Instead, the scaled profiles of the round ends of fairly bright stellar trails were measured and compared directly with those of the comets. The cometary profiles of 86P/Wild3 and 120P/Mueller 1 were identical within measurement errors to the scaled stellar profiles considering the faintness of each comet and the rms scatter of the sky background in each of the exposures. 86P/Wild3 and 120P/Mueller 1 were therefore considered as point sources. The apparent magnitude of 120P/Mueller 1 was 20.3 $\pm$ 0.2 which corresponds to a nuclear radius of 1.5 $\pm$ 0.2 km. Also $m_{\rm coma} \geq 20.76$, indicating that the nucleus dominates the observed flux and therefore the nuclear radius estimate for this comet is close to the real value. The measured apparent magnitudes, nuclear radii estimates and $m_{\rm coma}$ for 43P/Wolf-Harrington, 81P/Wild 2 and 86P/Wild 3 are listed in Table 3. A comparison of $m_{\rm coma}$ to the measured apparent magnitudes for these three comets shows that the dominant flux source remains uncertain.

Of the two images of 79P/du Toit-Hartley obtained, the comet was only partly visible on the 2nd frame due to a pointing error in the telescope. Although identification was possible, by its known rate of motion, only the first frame could be used for the photometry. Its apparent magnitude was 23.3 ± 0.4 corresponding to a nucleus radius of 1.4 $\pm$ 0.3 km. $m_{\rm coma}$ was calculated to be $\geq$ 21.55. Comparison of this value with the measured apparent magnitude again shows that the dominant flux source is uncertain.

3.3. Active comets

In this section the results and analysis for each comet shall be discussed separately and in more detail than the unresolved comets of the previous section. Again the analysis procedures used are similar for each comet. Therefore only the case of 119P/Parker-Hartley will be discussed fully.

3.3.1. 119P/Parker−Hartley

One image in each of the B, V, and R filters was taken of 119P/Parker-Hartley, each with an exposure time of 600s. An extensive dust coma was present. In the R frame the dust tail extended $\sim$ 20 arcsec, illustrating the degree of activity possible for short period comets at 3.42 AU. For all exposures of the active comets discussed in this section nearby stars and cosmic rays were removed. B, V and R magnitudes were measured through apertures of radius 8.6 arcsec and are listed in Table 4.

To measure the relative dust production rate the quantity $Af\rho$ is used, first defined by A'Hearn et al. (1984). $Af\rho$ is an aperture independent quantity which is roughly proportional to the dust production rate of a comet assuming equal size distri-

Table 5. $Af\rho$ values for the active comets. The following $Af\rho$ radius values are equivalent at the heliocentric distances of each comet listed in Table 1.

Comet	$Af\rho$ [cm]	$Af\rho$ radius [arcsec]	R Magnitude within $Af\rho$ radius	$m_{\rm coma}$ within $Af\rho$ radius	Profile gradient within $Af\rho$ radius*
119P/Parker−Hartley	74.7 ± 3.0	6.0	17.58 ± 0.04	18.15 ± 1.35	$-1.84 \pm 0.73^\dagger$
32P/Comas−Solá	38.6 ± 2.0	6.6	17.86 ± 0.06	18.65 ± 1.80	$-1.59 \pm 0.59^\dagger$
74P/Smirnova−Chernykh	228.8 ± 11.4	4.3	17.75 ± 0.05	17.97 ± 0.64	-1.49 ± 0.07
P/1993 K2 (Helin−Lawrence)	56.4 ± 3.6	4.0	19.46 ± 0.07	20.36 ± 1.63	-1.60 ± 0.12
9P/Tempel 1	12.0 ± 1.0	5.4	19.84 ± 0.10	20.57 ± 1.49	$-2.01 \pm 0.57^\dagger$
89P/Russell 2	5.9 ± 0.5	6.6	19.86 ± 0.12	21.79 ± 3.62	-1.30 ± 0.06
87P/Bus	7.4 ± 1.1	6.5	19.88 ± 0.16	20.52 ± 2.01	-1.34 ± 0.12

$\star$ Calculated by applying a least squares fit to the data points within the $Af\rho$ radii of the cometary profiles of Fig. 1, † Weighted least squares fit

Table 6. Preliminary and refined nuclear radii upper limit estimates for the active comets. See text.

Comet	R Magnitude within 9 pixel radius	Corresponding upper limit to nuclear radii [km]	R Magnitude of scaled PSF	Corresponding refined upper limit to nuclear radii [km]
119P/Parker−Hartley	17.97 ± 0.04	7.4 ± 0.2	19.31 ± 0.28	4.0 ± 0.6
32P/Comas−Solá	18.29 ± 0.04	5.5 ± 0.1	19.48 ± 0.26	3.2 ± 0.4
74P/Smirnova−Chernykh	18.07 ± 0.05	12.2 ± 0.3	19.24 ± 0.31	7.1 ± 1.1
P/1993 K2 (Helin−Lawrence)	19.67 ± 0.06	6.7 ± 0.2	21.23 ± 0.51	3.3 ± 0.9
9P/Tempel 1	20.15 ± 0.07	3.2 ± 0.1	20.87 ± 0.45	2.3 ± 0.5
89P/Russell 2	20.46 ± 0.09	2.0 ± 0.1	21.41 ± 0.47	1.3 ± 0.3
87P/Bus	20.52 ± 0.12	1.9 ± 0.1	22.21 ± 1.07	0.9 ± 0.5

butions of particles in the coma. $Af\rho$ [cm] can be determined from the observations using:

$$Af\rho = \frac{(2\Delta R_h)^2 F_{comet}}{\rho F_\odot} \quad (4)$$

where A is the geometric albedo of the cometary dust grains, the filling factor f is the total cross section of the grains in the field of view, ρ [cm] is the radius of the field of view, R_h[AU] and Δ[cm] are the heliocentric and geocentric distances respectively. $F_{comet}/F_\odot$ is the ratio of the cometary and solar flux at the observed wavelength. A value for ρ of 1.15×10^9 cm was used for all comets discussed in this section and determines the radius of the photometric aperture used in deriving an $Af\rho$ value. By measuring the R band magnitude within this radius the right hand side of Eq. (4) can be evaluated to yield an $Af\rho$ value for the comet. The R magnitude measured through an aperture of radius 6 arcsec was 17.58 ± 0.04 which corresponds to an $Af\rho$ value of 74.7 ± 3.0 cm (also listed in Table 5).

It should be noted that the quantity $Af\rho$ is not strictly applicable to a non steady-state coma, therefore whether or not the coma brightness can be represented by a steady-state coma model must be determined. Hence the surface brightness profile was calculated by measuring the flux from the comet within a series of circular annuli 1–4 pixels wide extending from 2–42 pixels. The resulting plot of surface brightness [mag./arcsec^2] vs. log(r)[arcsec] is dependent on the state of the coma (Jewitt 1991). Fig. 1a shows the surface brightness profile plot of 119P/Parker-Hartley. The two solid diagonal lines, with gradients of -1 and -1.5 represent steady state coma models. The steeper gradient takes into account the effects of radiation pressure (Jewitt & Meech 1987). The vertical line is the $Af\rho$ radius. Applying a weighted least squares fit to the data points within the $Af\rho$ radius gives a value of -1.84 ± 0.73 for the slope of the profile. Therefore a steady state coma model can be applied to this comet and the above $Af\rho$ value is feasible. Table 5 lists the profile gradients of all the active comets.

Unlike the comets of the previous section the quantity $\Sigma(r)$ of Eq. (2) can be evaluated for 119P/Parker-Hartley. As the surface brightness profile of 119P/Parker-Hartley can be represented by a steady state coma model Eq. (2) can be applied to 119P/Parker-Hartley to give $m_{\rm coma} = 18.15 \pm 1.35$ within the $Af\rho$ radius. The total apparent R magnitude within the $Af\rho$ radius was 17.58 ± 0.04 and any nucleus contribution to the calculated $Af\rho$ value is negligible.

To derive an upper limit to the nuclear radius of 119P/Parker-Hartley, it is not desirable to use a large aperture due to the overwhelming contribution from the dust coma. The apparent magnitude was hence measured through a circular aperture of radius 3 arcsec. This radius was chosen to minimise the coma contribution and yet include all flux from the nucleus, as here the intensity of the PSF becomes negligible. An R magnitude value of 17.97 ± 0.04 was found corresponding to an upper limit to the nuclear radius of 7.4 ± 0.2 km. As a way of refining this upper limit the PSF for the frame was scaled and subtracted from 119P/Parker-Hartley. The residual flux was measured and subtracted from the total flux from the comet to calculate the magnitude of the scaled PSF. The PSF magnitude for 119P/Parker-Hartley was 19.31 ± 0.28 corresponding to an upper limit of

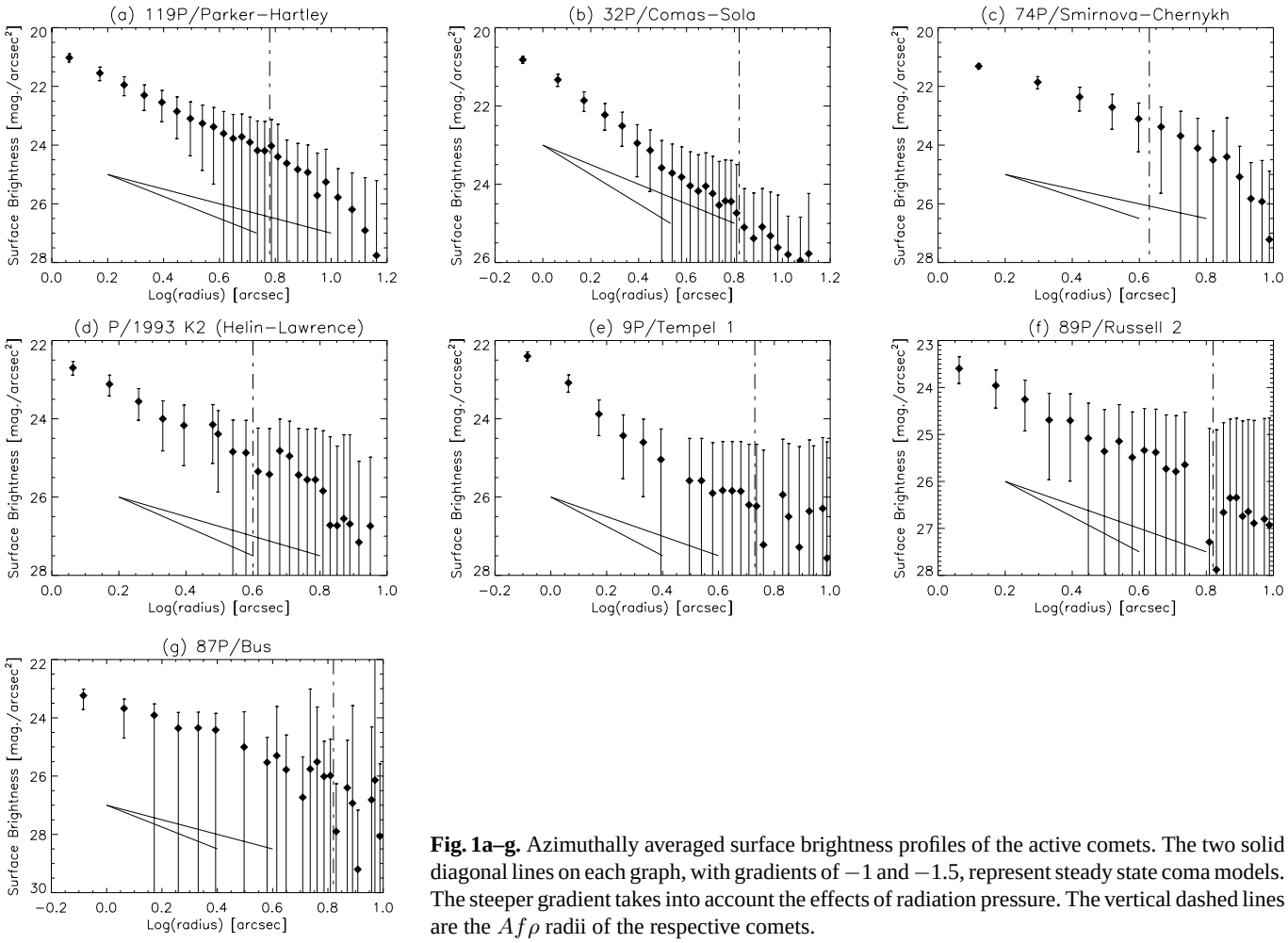

Fig. 1a–g. Azimuthally averaged surface brightness profiles of the active comets. The two solid diagonal lines on each graph, with gradients of -1 and -1.5, represent steady state coma models. The steeper gradient takes into account the effects of radiation pressure. The vertical dashed lines are the $Af\rho$ radii of the respective comets.

4.0 ± 0.6 km. Although the error in this new value is significantly larger the upper limit itself has been reduced by $\sim 46\%$. Both the preliminary and refined upper limits to the nuclear radius are listed in Table 6.

3.3.2. 32P/Comas−Solá

As in the case of 119P/Parker-Hartley only one image in each of the B, V, and R filters was taken, each with exposure times of 600s. In the R frame the dust tail extended ~ 10 arcsec. B, V, and R magnitudes for 32P/Comas-Solá were measured through apertures of radius 6.6 arcsec and are listed in Table 4. The R magnitude within a 6.6 arcsec radius aperture was 17.86 ± 0.06 which corresponds to an $Af\rho$ value of 38.6 ± 2.0 cm. The surface brightness profile was calculated by measuring the flux from the comet through a series of circular annuli 1–4 pixels wide extending from 2–40 pixels. The surface brightness profile for 32P/Comas-Solá is shown in Fig. 1b. A steady state coma is assumed for this comet and $m_{\rm coma} = 18.65 \pm 1.80$ within the $Af\rho$ radius. Therefore the dust coma dominates the observed flux within the $Af\rho$ radius. The R magnitude, measured through a 9 pixel radius aperture, was 18.29 ± 0.04. Corresponding to an upper limit to the nuclear radius of 5.5 ± 0.1 km. The scaled PSF magnitude, as described for 119P/Parker-Hartley, was 19.48 ± 0.26 reducing the upper limit to 3.2 ± 0.4 km.

3.3.3. 74P/Smirnova−Chernykh

4 images were taken of 74P/Smirnova-Chernykh, 2 with the R filter and 1 in each of the B, and V filters. Each had an exposure time of 300s. The R frames were shifted and coadded to give a combined image with an effective exposure time of 600s. 74P/Smirnova-Chernykh was by far the most active comet considered here. Even at a heliocentric distance of 4.61 AU a dust coma extending ~ 8.3 arcsec was observed in the R frame. The B, V and R magnitudes for 74P/Smirnova-Chernykh were measured through an aperture of radius 8.3 arcsec and are listed in Table 4. The R magnitude within an aperture of 4.3 arcsec radius was 17.75 ± 0.05 which gives an $Af\rho$ value of 228.8 ± 11.4 cm. The surface brightness profile was calculated by measuring the flux from the comet through a series of circular annuli 1–2 pixels wide extending from 2–30 pixels (Fig. 1c). This plot shows that a steady state coma model is viable for this comet. Therefore using Eq. (2) we find a modelled coma magnitude $m_{\rm coma}$ of 17.97 ± 0.64 within the $Af\rho$ radius. Comparison with the observed magnitude shows that the dust coma dominates the

$Af\rho$ measurement. The R magnitude measured through a 9 pixel radius aperture was 18.07 ± 0.05 giving an upper limit of 12.2 ± 0.3 km for the nuclear radius. The R magnitude of the scaled PSF was 19.24 ± 0.31 reducing the upper limit of 74P/Smirnova-Chernykh to 7.1 ± 1.1 km.

3.3.4. P/1993 K2 (Helin−Lawrence)

2 images in each of the B, V, and R filters was taken of Helin-Lawrence. All images with a common filter type were shifted and coadded to produce single B, V, and R images of Helin-Lawrence. The dust tail of Helin-Lawrence extended out to 14 arcsec in the R image. B, V, and R magnitudes measured through apertures of radius 6 arcsec are listed in Table 4. The R magnitude measured through an aperture of 4 arcsec was 19.46 ± 0.07 giving an $Af\rho$ value of 56.4 ± 3.6 cm. The surface brightness profile was calculated by measuring the flux from Helin-Lawrence through a series of circular annuli 1–2 pixels wide extending from 2–30 pixels (Fig. 1d). A steady state coma is assumed and $m_{\rm coma} = 20.36 \pm 1.63$. The R magnitude measured through a 9 pixel radius was 19.67 ± 0.06 corresponding to an upper limit of 6.7 ± 0.2 km for the nucleus radius. The R magnitude of the scaled PSF was 21.23 ± 0.51 reducing the upper limit to 3.3 ± 0.9 km.

3.3.5. 9P/Tempel 1

As in the case of 74P/Smirnova-Chernykh 4 images were taken of 9P/Tempel 1, 2 with the R filter and 1 in each of the B and V filters. The R frames were shifted and coadded. In each of the B, V, and R frames 9P/Tempel 1 was almost stellar in appearance. Only PSF subtraction revealed any sign of a faint coma. B, V, and R magnitudes measured through an aperture of radius 6.3 arcsec are listed in Table 4. The R magnitude measured through an aperture of radius 5.4 arcsec was 19.84 ± 0.10 giving an $Af\rho$ value of 12.0 ± 1.0 cm. The surface brightness profile was calculated using the same procedure used for 74P/Smirnova-Chernykh and Helin-Lawrence (Fig. 1e). $m_{\rm coma} = 20.57 \pm 1.49$ within the $Af\rho$ radius. The R magnitude measured within a 9 pixel radius aperture was 20.15 ± 0.07 giving an upper limit of 3.2 ± 0.1 km for the nucleus radius. The R magnitude of the scaled PSF was 20.87 ± 0.45 reducing the upper limit to 2.3 ± 0.5 km.

3.3.6. 89P/Russell 2

Only V and R filter images were taken of 89P/Russell 2, each with exposure times of 900s. The 2 R filter images were shifted and coadded to give a single image with an effective exposure time of 1800s. Similar to the case of 9P/Tempel 1, PSF subtraction revealed a faint coma around the comet and R and V magnitudes measured through circular apertures of radius 7.3 arcsec are listed in Table 4. The R magnitude measured through an aperture of radius 6.6 arcsec was 19.86 ± 0.12 giving an $Af\rho$ value of 5.9 ± 0.5 cm. The surface brightness profile was calculated by measuring the flux within a series of circular annuli 1–3 pixels wide extending from 2–30 pixels (see Fig. 1f). A steady state coma is assumed for 89P/Russell 2 and $m_{\rm coma} = 21.79 \pm 3.62$ within the $Af\rho$ radius. Although 89P/Russell 2 is nearly a point source the large uncertainty in $m_{\rm coma}$ suggests the dust coma could dominate the observed flux. The R magnitude measured within a 9 pixel radius aperture was 20.46 ± 0.09 giving an upper limit of 2.0 ± 0.1 km for the nucleus radius. The R magnitude of the scaled PSF was 21.41 ± 0.47 reducing the upper limit to 1.3 ± 0.3 km.

3.3.7. 87P/Bus

Similar to 89P/Russell 2 only R and V images were taken of 87P/Bus, but the exposure times here were 300s. Each image with a common filter type was shifted and coadded to give single R and V images. Even in the coadded R image the comet was extremely faint. R and V magnitudes measured through apertures of radius 6.9 arcsec are listed in Table 4. The R magnitude measured through an aperture of 6.5 arcsec was 19.88 ± 0.66 giving an $Af\rho$ value of 7.4 ± 1.1 cm. The surface brightness profile was calculated using the same procedure used for 89P/Bus (Fig. 1g). A steady state coma is assumed and $m_{\rm coma} = 20.52 \pm 2.01$ within the $Af\rho$ radius. Therefore the dust coma dominates the observed flux. The R magnitude measured within a 9 pixel radius aperture was 20.52 ± 0.12 giving an upper limit of 1.9 ± 0.1 km for the nucleus radius. The R magnitude of the scaled PSF was 22.21 ± 1.07 reducing the upper limit to 0.9 ± 0.5 km.

4. Discussion

4.1. Nuclear radii estimates

The nuclear radii estimates for the inactive comets listed in Table 3 may well be extremely close to the actual values[2] as no evidence for activity was found. Strictly speaking however, the majority could be upper limits as the presence of an unresolved faint coma cannot be ruled out when one considers that these comets were observed at heliocentric distances within the water sublimation region. Also the CLICC Atlas of Cometary Lightcurves (Kamél 1992) shows that at these distances most cometary lightcurves do not correspond to those of point source objects of constant scattering cross–section (i.e. inert cometary nuclei). For the active comets listed in Table 6, the upper limits derived for the cometary nuclei without using the PSF subtraction technique discussed in Sect. 3.3.1 may be regarded as firm. For the smaller upper limits obtained using PSF subtraction, in some cases the 3σ upper limit is the same as or exceeds the more simple analyses. More realistic modelling might be achieved by convolving the PSF with a steady state coma model and adjusting it to the data (Lamy & Toth et al. 1995), but unfortunately to be successful requires a higher signal to noise ratio than was available to us. We note that the nuclear radii estimates listed in Tables 3 & 6 are typical for Jupiter family comets. The nuclear radii estimates derived in this paper significantly increase the

[2] Assuming an albedo of 0.04.

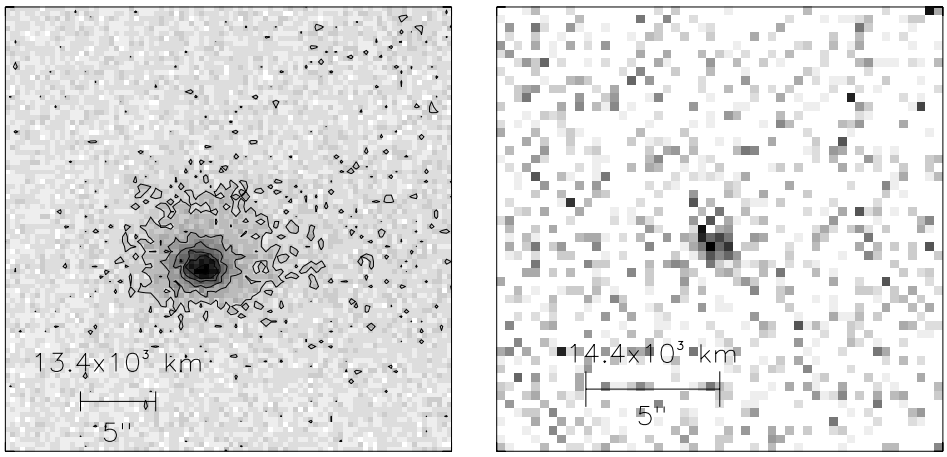

Fig. 2. R band CCD Images of 74P/Smirnova-Chernykh (left) and 81P/Wild 2 (right) at heliocentric distances of 4.61 AU and 4.25 AU respectively, illustrating the range of activity possible for comets at large heliocentric distances.

number of such estimates for short period comets published to date. A more statistically useful sample is therefore obtained.

Column 3 of Table 7 lists previously measured nuclear radii estimates and lower limits along with lower limits derived in this paper using published H_2O production rates and active nuclear areas. The lower limit estimates for 9P/Tempel 1 and 81P/Wild 2 stated in Osip et al. (1992) were derived by assuming a spherical nucleus and 100% of the surface area of the nucleus is active to produce the measured OH production rates. For 87P/Bus, 74P/Smirnova-Chernykh, 69P/Taylor and 43P/Wolf-Harrington the amount of active area required to produce the measured OH production rates given in A'Hearn et al. (1995) were used to derive lower limits to their nuclear radii. Again a spherical nucleus and 100% active surface area is assumed. A value of 0.46 km^2 for the amount of active area normal to the sun at 205 K required to produce the observed water (Newburn & Spinrad 1989) was used to calculate a lower limit to the nuclear radius of 86P/Wild 3. A spherical nucleus is assumed but this time 100% of the area normal to the sun is assumed to be active. For 26P/Grigg-Skjellerup a lower limit of $\geq$ 0.38 km was derived using the published H_2O production rate (Jockers et al. 1993; Johnstone et al. 1993). The amount of active area required to produce the measured H_2O at a heliocentric distance of 1.01 AU was calculated using a Sublimating Nucleus Model based on the equations of Meech et al. (1986). By assuming a spherical nucleus and the entire surface is active the lower limit value was reached.

The lower limits listed in Table 7 derived by these methods are less than, or as in the case of 87P/Bus equal to, our estimates. A value of 2.0 $\pm$ 0.3 km for the radius of 81P/Wild 2 is in excellent agreement with the previous value of 2.0 km (Meech 1998). However, the radius estimates for 86P/Wild 3 & 26P/Grigg-Skjellerup of 1.1 $\pm$ 0.2 km and $\leq$ 1.2 $\pm$ 0.1 km respectively are considerably smaller than the previous estimates of 3.10 km & 2.9 km (Meech 1998). Recently the nucleus of 9P/Tempel 1 was detected with the Hubble Space Telescope at a heliocentric range of 4.48 AU (Lamy 1998). The nucleus is elongated with semi-axes $a = 3.9$ km and $b = 2.8$ km (for an assumed albedo of 4%). This is in excellent agreement with the value obtained here of $\leq 2.3 \pm 0.5$ km within the measurement error. In our observations 9P/Tempel 1 displayed coma activity and therefore its nuclear radius upper limit was obtained by the method described in Sect. 3.3.1. The agreement with Lamy (1998) shows that the method of refining the nuclear radii upper limits mentioned in Sect. 3.3.1 can be effective in achieving a radius value extremely close to the actual value.

4.2. Fractional active area

The lower limits to the nuclear radii listed in Column 3 of Table 7 were used to derive lower limits to the percentage of active nucleus area (F) at the time the observations of previous studies were taken. Taking 9P/Tempel 1 as an example, a lower limit of $\geq$ 1.25 km for the nucleus radius was found by Osip et al. (1992). As mentioned earlier this previous value was originally derived from the amount of active area required to produce the measured OH production rates. The amount of active area is compared to the maximum nucleus surface area possible derived from our value of $\leq 2.3 \pm 0.5$ km for the nuclear radius. By assuming a spherical nucleus a lower limit for F of $\geq 19.9\%$ is derived. Similarly the F values for 81P/Wild 2, 86P/Wild 3, 26P/Grigg-Skjellerup, 87P/Bus, 74P/Smirnova-Chernykh, 69P/Taylor and 43P/Wolf-Harrington were also calculated and are given in Table 7. The values obtained for 9P/Tempel 1, 81P/Wild 2 and 87P/Bus are unusually high compared with the distribution of percentage active areas presented if Fig. 6 of A'Hearn et al. (1995). Of the comets studied by A'Hearn et al. the percentage of active areas ranged from $\sim$ 0–16.5% for periodic comets. It is therefore apparent that estimates of fractional active areas are continuing to increase as more nuclear radii estimates emerge.

4.3. $Af\rho$ measurements

Roughly 50% of the comets observed here displayed coma activity. This is a significantly large fraction for comets in the heliocentric range of 3 AU $\leq R_h \leq$ 6 AU even with a sample of just 15 comets. Fig. 2 illustrates the difference in activity for 2 of these 15 comets at similar heliocentric distances. Fig. 3 is plot of the $Af\rho$ values given in Table 5 vs. heliocentric distance. The

Table 7. Comparison of nuclear radii estimates with previous values.

Comet	Nuclear radii [km]	Previous values$^{\diamond}$ [km]	Ref.	F* [%]	R$_h$ [AU]
9P/Tempel 1	$\leq 2.3 \pm 0.5$	≥ 1.25	2	≥ 19.9	1.52–2.05
81P/Wild 2	2.0 ± 0.3	≥ 1.25	2	≥ 29.5	1.49–2.62
		2.00	3		
86P/Wild 3	1.1 ± 0.2	3.10	3		
		≥ 0.38	4	≥ 8.5	2.41
26P/Grigg−Skjellerup	$\leq 1.2 \pm 0.1$	2.90	3		
		≥ 0.35	6,7	≥ 7.3	1.01
32P/Comas−Solá	$\leq 3.2 \pm 0.4$	$0.99^{\dagger}$	5		
		$1.15^{\ddagger}$	5		
87P/Bus	$\leq 0.9 \pm 0.5$	≥ 0.90	1	≥ 41.3	3.15
74P/Smirnova−Chernykh	$\leq 7.1 \pm 1.1$	≥ 1.70	1	≥ 4.3	3.56
69P/Taylor	3.6 ± 0.7	≥ 0.25	1	≥ 0.3	1.96
43P/Wolf−Harrington	3.3 ± 0.7	≥ 0.42	1	≥ 1.1	1.82

$\diamond$ The lower limits are either directly given, or based on other information, in the respective references. See text. $*$ The minimum percentage of active nucleus area at the time of previous measurements, † & ‡ Equatorial & Polar radii respectively. Based on nucleus precession model by Whipple & Sekanina (1979). **References:** [1] A'Hearn et al. (1995), [2] Osip et al. (1992), [3] Meech (1998), [4] Newburn & Spinrad (1989), [5] Sekanina (1985), [6] Johnstone et al. (1993), [7] Jockers et al. (1993)

Table 8. Comparison of $Af\rho$ values with previous values listed in A'Hearn et al. (1995).

Comet	$Af\rho$ [cm]	R [AU]	Previous $Af\rho$ value [cm]	R[AU]
9P/Tempel 1	12.0 ± 1.0	$3.51^{\dagger}$	263.0	$1.52–2.05^{\dagger}$
74P/Smirnova−Chernykh	228.8 ± 11.4	$4.61^{\ddagger}$	602.6	$3.56^{\star}$
87P/Bus	7.4 ± 1.1	$3.38^{\ddagger}$	16.2	$2.23^{\dagger}$
			251.2	$3.15^{\ddagger}$
81P/Wild 2	≤ 12.1	$4.25^{\dagger}$	169.8	$2.23^{\dagger}$
43P/Wolf−Harrington	≤ 28.4	$4.87^{\dagger}$	131.8	$1.82^{\dagger}$

† Pre-perihelion, $\star$ At perihelion, ‡ Post-perihelion

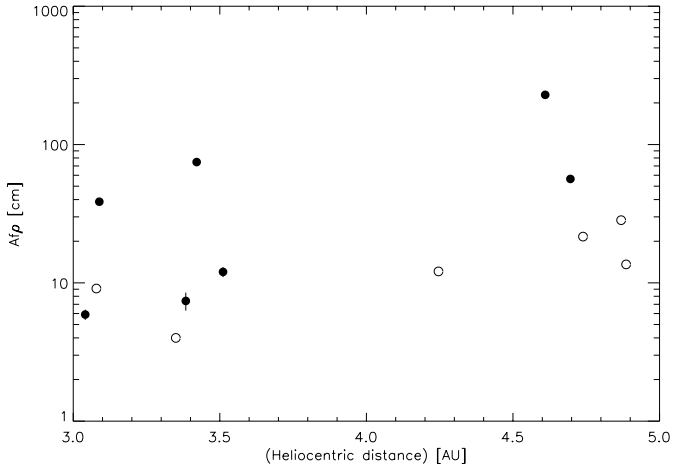

Fig. 3. A plot of $Af\rho$ [cm] vs. Heliocentric distance [AU] for the comets of Sect. 3.2 (open circles) & 3.3 (filled circles). The open circles are upper limits.

plot reveals that many comets may maintain large $Af\rho$ values out to 5 AU. Any nucleus contribution to the $Af\rho$ values for the active comets is considered negligible after comparison of the R magnitudes measured within the $Af\rho$ radii with (a) the derived $m_{\rm coma}$ measurement for each comet within the $Af\rho$ radii, and (b) the scaled PSF R band magnitudes listed in Table 6. Taking 74P/Smirnova-Chernykh as an example, its scaled PSF R magnitude was 19.24 ± 0.31 and the R magnitude measured within the $Af\rho$ radius was 17.75 ± 0.05. Therefore a maximum of $\sim$ 20% of the total flux within the $Af\rho$ radius could be due to the nucleus. As an unresolved coma may indeed be present for the comets of Sect. 3.2 Fig. 3 also includes upper limits to their dust production rates using the $m_{\rm coma}$ values listed in Table 3. Although some of these $Af\rho$ upper limits are quite high they can only be regarded as evidence for possible activity as the flux observed from the comets of Sect. 3.2 could be due to the bare nuclei only.

Table 8 compares the present $Af\rho$ values with those listed in A'Hearn et al. (1995) derived at different heliocentric distances. 9P/Tempel 1 shows a dramatic decrease in dust production over a

change in R_h of ~ 1.73 AU. 74P/Smirnova-Chernykh undergoes a shallower rate of change of dust production with heliocentric distance which is typical of dynamically new comets (A'Hearn et al. 1995). If 74P/Smirnova-Chernykh was a recent arrival to the inner solar system, compared to most other Jupiter family comets, this might explain how it can maintain its high degree of activity throughout its orbit given the high mass loss rate due to continuous sublimation of surface volatiles. 74P/Smirnova-Chernykh also displays the highest degree of activity observed by us with an $Af\rho$ value 228.8 ± 11.4 cm at 4.61 AU. With an aphelion distance of 4.81 AU it is apparent that this comet probably remains highly active throughout its entire orbit. Another candidate for continuous substantial outgassing throughout the orbit is P/Helin-Lawrence with an aphelion distance of 5.85 AU. A reasonably high $Af\rho$ measurement of 56.4 ± 3.6 cm (at $R_h = 4.69$ AU) was obtained.

An $Af\rho$ value of 7.4 ± 1.1 cm was measured for 87P/Bus at a post-perihelion distance of 3.38 AU. $Af\rho$ measurements for previous apparitions were 16.2 cm at a pre-perihelion distance of 2.23 AU and 251.2 cm at a post-perihelion distance of 3.15 AU. A'Hearn et al. (1995) found that for the majority of comets the production of dust as a function of position in an orbit remains the same from one orbit to the next, but this is clearly not the case for 87P/Bus. The post-perihelion $Af\rho$ values measured on different orbital passages are extremely different even though the comet is in approximately the same orbital position in each case. The post-perihelion dust production rate at $R_h = 3.15$–3.38 AU has decreased dramatically with each new orbital passage. As no recent gravitational perturbation of the comets orbit has occurred, the previous high post-perihelion activity may have been due to an outburst on the surface of the nucleus. Future $Af\rho$ measurements are necessary to further understand the erratic behaviour of 87P/Bus. Finally, we note that 81P/Wild 2 and 43/Wolf-Harrington show a huge decrease in dust production with increasing heliocentric distance, similar to 9P/Tempel 1.

4.4. Dust colours

From the (B–V) and (V–R) values listed in Table 4 it is apparent that the dust comae of 119P/Parker-Hartley, 32P/Comas-Solá, 74P/Smirnova-Chernykh and 89P/Bus show red colours relative to the sun. The $(B–V)_\odot$ and $(V–R)_\odot$ values are 0.67 (Tedesco et al. 1982) and 0.36 (Meech et al. 1995) respectively. Previous $(B-V)$ measurements for 74P/Smirnova-Chernykh are 0.86 ± 0.02 at $R_h = 3.559$ AU and 0.93 ± 0.02 at $R_h = 3.56$ AU (Remillard & Jewitt 1985). These are in excellent agreement with our measurement of 0.99 ± 0.16 and shows that there is no significant change in the colour of the ejected dust coma after several perihelion passages. The colour indices for 9P/Tempel 1 are similar to those of the sun, within the measurement error. P/Helin-Lawrence shows a blue colour at short wavelengths but is much redder at longer wavelengths when compared to the sun. A (V–R) value of -0.11 ± 0.21 was obtained for 87P/Bus. The fact that the V band magnitude is less than the R band magnitude for this comet may have been due to contamination by C_2 emissions within the passband of the V filter. Finally, no correlation of dust colour with heliocentric distance, phase angle or $Af\rho$ value was found. The lack of correlation of colour with heliocentric distance is consistent with previous studies by Jewitt & Meech (1986) and Jewitt & Meech (1988).

5. Summary

The nuclear radii estimates derived here for an assumed albedo of 0.04 range from $0.9 < r_N < 7.1$ km, which is typical for previously observed short period comets. After comparison of these estimates with previous observations it was possible to derive lower limits to the fraction of active area at the time the previous observations were taken. Unusually high values of $\geq 19.9\%$, $\geq 29.5\%$ and $\geq 41.3\%$ were found for 9P/Tempel 1, 81P/Wild 2 and 87P/Bus respectively. The other lower limits derived ranged from 0.3–8.5%. Roughly 50% of the comets observed displayed activity, with $Af\rho$ values ranging from 5.9–228.8 cm. In certain cases such as 74P/Smirnova-Chernykh the observed activity was substantial and probably continuous throughout its entire orbit. Comparison of previous $Af\rho$ values with those derived here for 87P/Bus reveal that the production of dust as a function of position in its orbit is not the same from one orbit to the next. No correlation of dust colour with heliocentric distance was found, which is consistent with previous studies.

Acknowledgements. The Jacobus Kapteyn Telescope is operated on the island of La Palma by the Royal Greenwich Observatory at the Spanish Observatorio del Roque de los Muchachos of the Instituto de Astrofísica de Canarias. The authors would like to thank the referee Olivier Hainaut for his constructive comments and suggestions for the first draft of this paper. Financial assistance from DENI is gratefully acknowledged.

References

A'Hearn M.F., Schleicher D.G., Feldman P.D., Millis R.L., Thompson D.T., 1984, AJ 89, 579
A'Hearn M.F., Millis R.L., Schleicher D.G., Osip D.J., Birch P.V., 1995, ICARUS 118, 223
Bus S.J., A'Hearn M.F., Bowell E., Stern S.A., 1998, ICARUS, in press
Davis L.E., 1989, A Reference Guide to the IRAF/APPHOT Package. NOAO, Tucson, Arizona
Davis L.E., 1994, A Reference Guide to the IRAF/DAOPHOT Package. NOAO, Tucson, Arizona
Fitzsimmons A., Dahlgren M., Lagerkvist C.I., Magnusson P., Williams I.P., 1994, A&A 282, 634
Hainaut O.R., West R.M., Smette A., Marsden B.G., 1994, A&A 289, 311
Hainaut O.R., Meech K.J., Boehnhardt H., West R.M., 1998, A&A 333, 746
Jewitt D.C., Danielson G.E., 1984, ICARUS 60, 435
Jewitt D.C., Meech K.J., 1986, ApJ 310, 937
Jewitt D.C., Meech K.J., 1987, ApJ 317, 992
Jewitt D.C., Meech K.J., 1988, AJ 96, 1723
Jewitt D.C., 1991, Cometary Photometry. In: Newburn R.L. Jr., Neugebauer M., Rahe J. (eds.) Comets in the Post-Halley Era. Vol.1. Kluwer, Dordrecht, p. 19
Jockers K., Kiselev N.N., Boehnhardt H., Thomas N., 1993, A&A 268, L9

Johnstone A.D., Coates A.J., Huddleston D.E., et al., 1993, A&A 273, L1
Kamél L., 1992, A&AS 92, 85
Lamy P., Toth I., 1995, A&A 293, L43
Lamy P., 1998, IAU Circ., 7000
Landolt A.U., 1992, AJ 104, 340
Luu J.X., Jewitt D.C., 1992, AJ 104, 2243
Luu J.X., 1993, ICARUS 104, 138
Massey P., 1997, A User's Guide to CCD Reductions with IRAF. NOAO, Tucson, Arizona
McNaught R.H., Cass C.P., 1995, IAU Circ., 6198
Meech K.J., Jewitt D.C., Ricker G.R., 1986, ICARUS 66, 561
Meech K.J., 1994, Urey Prize Lecture
Meech K.J., Knopp G.P., Farnham T.L., 1995, ICARUS 116, 46
Meech K.J., Hainaut O.R., 1997, IAU Joint Discussion on Interactions between Planets and Small Bodies
Meech K.J., 1998, In: Asteroids, Comets, Meteors 1996, COSPAR Colloquium 10, in press
Mueller B.E.A., 1992, In: Harris A., Bowell E. (eds.) Asteroids, Comets, Meteors 1991, 425
Newburn R.L., Spinrad H., 1989, AJ 97, 552
Osip D.J., Scheicher D.G., Millis R.L., 1992, ICARUS 98, 115
Remillard R.A., Jewitt D.C., 1985, ICARUS 64, 27
Russell H.N., 1916, ApJ 43, 173
Sekanina Z., 1985, AJ 90, 1370
Tancredi G., Lindgren M., 1994, ICARUS 107, 311
Tedesco E.F., Tholen D.J., Zellner B., 1982, AJ 87, 1585
Whipple F.L., Sekanina Z., 1979, AJ 84, 1894